J. Phys. Chem. A **2003,** *107,* 6055−6061

Direct Dynamics Study on the Hydrogen Abstraction Reaction $N_2H_4 + H \rightarrow N_2H_3 + H_2$

Qian Shu Li,* Xin Zhang, and Shao Wen Zhang

School of Science, Beijing Institute of Technology, Beijing 100081, People's Republic of China

Received: March 7, 2003; In Final Form: June 8, 2003

A direct ab initio dynamics method has been employed to investigate the hydrogen abstraction reaction $N_2H_4 + H \rightarrow N_2H_3 + H_2$, which is predicted to have four possible reaction channels caused by different structures of N_2H_4 and different positions of hydrogen atom attack. The structures and frequencies at the stationary points and along the minimum energy paths (MEPs) are determined using the UMP2/6-31+G(d,p) method. Energetic information is further refined at the PMP4/6-311+G(3df,2pd)//UMP2/6-31+G(d,p) level of theory. The rate constants are calculated using the improved canonical variational transition state theory with the small-curvature tunneling correction (ICVT/SCT) in the temperature range of 220−3000 K. The calculated results show that in the lower-temperature range, the most favorable reaction channels are reaction 1 [N_2H_4(a) + H → TS(a1) → N_2H_3(a) + H_2] and reaction 3 [N_2H_4(b) + H → TS(b1) → N_2H_3(b) + H_2], while in the higher-temperature range, reaction 2 [N_2H_4(a) + H → TS(a2) → N_2H_3(a) + H_2] and reaction 4 [N_2H_4(b) + H → TS(b2) → N_2H_3(b) + H_2] become more important. The calculated total rate constants of the four reaction channels are in good agreement with the available experimental data.

Introduction

Hydrazine (N_2H_4), methylhydrazine (CH_3NHNH_2), and unsymmetrical dimethylhydrazine [$(CH_3)_2NNH_2$] are at present attracting growing interest as an important class of diamine-based rocket fuels.[1] These propellants are typically oxidized by nitrogen tetroxide (N_2O_4) in rocket motors to generate the desired thrust for the Titan launch vehicles and the space shuttle as well as other spacecrafts in low earth orbit (LEO).[2] Especially as a monopropellant, N_2H_4 is also very common in small attitude and trajectory control systems of many satellites.

Hydrazine is one of the rare endothermic compounds, whose decomposition can lead to self-ignition[3−6] or detonation,[6−8] or it can be stabilized as a flame without any oxidizer. To accurately model the combustion of N_2H_4, either the decomposition mechanisms or the kinetics of the reactions that are involved are required. But only some initial decomposition reaction rates[10−13] and a few rate constants for hydrazine reacting with atoms and radicals[9,14−21] have been measured. The reaction of atomic hydrogen with hydrazine is one such reaction. This reaction is very important because it is one of the chain propagation steps in the flame and pyrolytic decomposition of N_2H_4[17] and can provide an uncomplicated probe of chemical reactivity. According to the investigation of Schiavello and Volpio,[19] the reaction of an H atom with N_2H_4 can proceed via a hydrogen atom abstraction reaction

$$H + N_2H_4 \rightarrow N_2H_3 + H_2$$

Birse and Melville[18] proposed another possible pathway for this reaction involving N−N bond fission in hydrazine

$$H + N_2H_4 \rightarrow NH_3 + NH_2$$

However, the latter reaction has proven to be of minor importance compared with the first reaction.[15,16,21,22]

Many investigations[16,19−24] into the reaction $H + N_2H_4 \rightarrow N_2H_3 + H_2$ have been reported over the past 40 years, and there have been several gas-phase reaction rate constant determinations[16,19−23] that cover a combined temperature range of 222−657 K. In a recent work, Vaghjiani et al.[23] acquired the Arrhenius expression $k_1 = (11.7 \pm 0.7) \times 10^{-12} \exp[-(1260 \pm 20)/T]$ cm^3 molecule^{-1} s^{-1}, but to the best of our knowledge, few theoretical calculations have been performed for this reaction.

In the study presented here, we report a direct ab initio dynamics[25] study on the abstraction of an H atom from hydrazine. For N_2H_4, there are two equivalent molecular structures with C_2 symmetry, which have been determined experimentally by Kohata et al.[38] We have considered all the reaction possibilities caused by different N_2H_4 isomers and different positions of hydrogen atom attack.

Computational Methods

A. Improved Canonical Variational Transition State Theory. The rate constant calculations are carried out by employing POLYRATE version 8.2.[32] For the purpose of comparison, calculations of the reaction rate constants are carried out by using the conventional transition state theory (TST) and the improved canonical variational transition state theory (ICVT).[26] By treating the threshold region as accurately as in the microcanonical variational theory, one can express the ICVT as

$$k^{\mathrm{IGT}}(T,s) = [h\Phi^{\mathrm{R}}(T)]^{-1}\int_{V^{\mathrm{AG}}}^{\infty} \mathrm{d}E\mathrm{e}^{-\beta}EN^{\mathrm{GT}}(E,s)$$

where $k^{\mathrm{IGT}}(T,s)$ is the improved generalized transition state theory rate constant, $\Phi^{\mathrm{R}}(T)$ is the partition function per unit length for reactants, $N^{\mathrm{GT}}(E,s)$ is the quantized cumulative reaction probability, β is equal to $(1/k_{\mathrm{B}}T)$, in which k_{B} is Boltzmann's constant, and V^{AG} is the maximum of the ground state vibrationally adiabatic potential curve. The ICVT dividing

---

* To whom correspondence should be addressed. Fax: +86-10-68912665. E-mail: qsli@bit.edu.cn.

10.1021/jp034592u CCC: $25.00

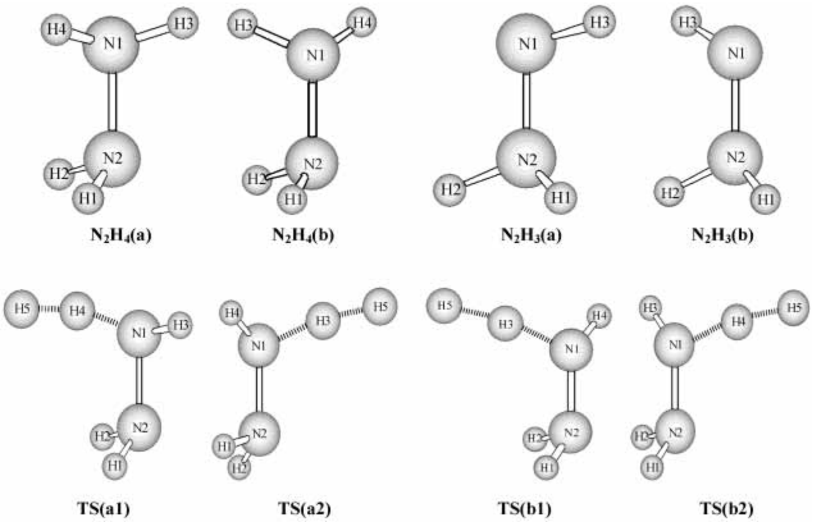

Figure 1. Conformations of stable stereoisomers of N_2H_4 and N_2H_3 and structures of possible transition states for the title reaction. See Tables 1 and 2 for the complete list of geometrical parameters.

surface is placed to minimize the improved generalized transition state theory rate constant

$$\frac{\partial k^{\mathrm{IGT}}(T,s)}{\partial s}\Big|_{s=s^{*\mathrm{ICVT}}(T)} = 0$$

Furthermore, the ICVT rate constants are also corrected with the small curvature tunneling (SCT) correction method proposed by Truhlar and co-workers,[33,34] which is based on the centrifugal dominant small curvature semiclassical ground state (CD-SCSAG) method.

B. Electronic Structure Calculations. By means of the GAUSSIAN98 program,[27] ab initio calculations are carried out for stationary points (reactants, transition states, and products) and for the minimum energy paths (MEPs) in an effort to obtain electronic structure information for the reactions. The geometries of the stationary points are fully optimized by employing the second-order unrestricted Møller−Plesset perturbation method (UMP2) with the 6-31+G(d,p) basis set.[28,29] The frequencies are calculated at the same level. Meanwhile, the QCISD/6-311G(d,p)[30] method is also used to calculate the stationary point properties of the reactions for comparison. The minimum energy paths (MEPs) are obtained at the UMP2/6-31+G(d,p) level of theory from $s = -1.80$ to 1.80 amu$^{1/2}$ b using the intrinsic reaction coordinate (IRC) method with a step size of 0.02 amu$^{1/2}$ b in mass-weighted Cartesian coordinates. The harmonic vibrational frequencies as well as the Hessian matrixes at the selected points along the MEPs are calculated at the same level. The spin-projected fourth-order Møller−Plesset perturbation theory (PMP4)[31] is employed using the 6-311+G(3df,2pd) basis set [PMP4/6-311+G(3df,2pd)// UMP2/6-31+G(d,p)] to refine the energies of stationary points and the selected points along the MEPs. In addition, the single-point energy calculations for stationary points are also carried out at the G2//QCISD/6-311G(d,p) level of theory for comparison.

Results and Discussion

It has been shown experimentally and theoretically that there are only two stable stereoisomers in hydrazine molecule N_2H_4[35−38] (Figure 1). Since there are two types of hydrogen atoms in each isomer of N_2H_4, there are correspondingly four different transition states (Figure 1) and four different possible reaction channels for the title reaction. In this study, we have reported all the possible channels and the species involved.

TABLE 1: Optimized Geometrical Parameters (distances in Å and angles in deg) of All the Reactants and Products at the UMP2/6-31+G(d,p) and QCISD/6-311G(d,p) Levels

	geometrical parameter	UMP2/ 6-31+G(d,p)	QCISD/ 6-311G(d,p)	exptl[a]
N_2H_4(a)	r(N2−N1)	1.434	1.437	1.449
	r(N2−H1)	1.015	1.017	1.021
	r(N2−H2)	1.012	1.013	1.021
	θ(N1−N2−H1)	112.3	111.2	112
	θ(N1−N2−H2)	107.5	106.6	106
	θ(H1−N2−H2)	108.5	106.8	106[b]
	Φ(H2−N2−N1−H4)	90.9	89.4	91
N_2H_4(b)	r(N2−N1)	1.434	1.437	1.449
	r(N2−H1)	1.012	1.013	1.021
	r(N2−H2)	1.015	1.017	1.021
	θ(N1−N2−H1)	107.5	106.6	106
	θ(N1−N2−H2)	112.3	111.2	112
	θ(H1−N2−H2)	108.5	106.8	106
	Φ(H2−N2−N1−H4)	90.9	89.4	91
H_2	r(H−H)	0.734	0.743	0.741
N_2H_3(a)	r(N2−N1)	1.350	1.362	
	r(N2−H1)	1.012	1.014	
	r(N2−H2)	1.008	1.010	
	r(N1−H3)	1.021	1.025	
	θ(N1−N2−H1)	120.7	118.3	
	θ(N1−N2−H2)	113. 6	111.8	
	θ(H1−N2−H2)	115.1	112.7	
	θ(N2−N1−H3)	105.5	104. 5	
	Φ(H1−N2−N1−H3)	25.5	32.1	
N_2H_3(b)	r(N2−N1)	1.350	1.362	
	r(N2−H1)	1.008	1.010	
	r(N2−H2)	1.012	1.014	
	r(N1−H3)	1.021	1.025	
	θ(N1−N2−H1)	113.5	111.8	
	θ(N1−N2−H2)	120.7	118.3	
	θ(H1−N2−H2)	115.1	112.7	
	θ(N2−N1−H3)	105.5	104.5	
	Φ(H2−N2−N1−H3)	25.6	32.1	

[a] From ref 38. [b] From ref 40.

A. Stationary Points. The optimized geometric parameters of all the reactants, products, and transition states at the UMP2/6-31+G(d,p) and QCISD/6-311G(d,p) levels along with the available experimental data[38−40] are given in Tables 1 and 2. The conformations of the main stationary points are also shown in Figure 1. From the results listed in Table 1, it can easily be seen that the optimized geometries for N_2H_4(a) and N_2H_4(b)

TABLE 2: Optimized Geometrical Parameters (distances in Å and angles in deg) of the Transition State Structures at the UMP2/6-31+G(d,p) and QCISD/6-311G(d,p) Levels[a]

	geometrical parameter	UMP2/ 6-31+G(d,p)	QCISD/ 6-311G(d,p)
TS(a1)	*r*(N2−N1)	1.397	1.409
	r(N2−H1)	1.017	1.018
	r(N2−H2)	1.011	1.013
	r(N1−H3)	1.021	1.020
	r(N1−H4)	1.192	1.141
	r(H4−H5)	0.979	1.082
	θ(N1−N2−H1)	114.9	112.8
	θ(N1−N2−H2)	109.0	107.7
	θ(N2−N1−H3)	106.6	106.1
	θ(N2−N1−H4)	111.8	111.3
	θ(H3−N1−H4)	102.0	102.1
	θ(H5− H4−N1)	166.6	160.9
	Φ(H5−H4−N1−N2)	47.8	47.8
TS(a2)	*r*(N2−N1)	1.404	1.420
	r(N2−H1)	1.011	1.013
	r(N2−H2)	1.010	1.013
	r(N1−H3)	1.200	1.155
	r(N1−H4)	1.022	1.022
	r(H3−H5)	0.965	1.050
	θ(N1−N2−H1)	114.4	111.5
	θ(N1−N2−H2)	109.0	107.0
	θ(N2−N1−H3)	107.3	106.7
	θ(N2−N1−H4)	108.4	107.8
	θ(H3−N1−H4)	100.0	99.8
	θ(H5−H3−N1)	167.5	164.1
	Φ(H5−H3−N1−N2)	47.9	47.9
TS(b1)	*r*(N2−N1)	1.397	1.409
	r(N2−H1)	1.011	1.013
	r(N2−H2)	1.017	1.018
	r(N1−H3)	1.192	1.141
	r(N1−H4)	1.021	1.020
	r(H3−H5)	0.979	1.082
	θ(N1−N2−H1)	109.0	107.7
	θ(N1−N2−H2)	114.9	112.8
	θ(N2−N1−H3)	111.8	111.3
	θ(N2−N1−H4)	106.6	106.1
	θ(H3−N1−H4)	102.0	102.1
	θ(H5− H3−N1)	166.6	160.9
	Φ(H5−H3−N1−N2)	47.8	47.8
TS(b2)	*r*(N2−N1)	1.404	1.420
	r(N2−H1)	1.010	1.013
	r(N2−H2)	1.011	1.013
	r(N1−H3)	1.022	1.022
	r(N1−H4)	1.200	1.155
	r(H4−H5)	0.965	1.050
	θ(N1−N2−H1)	109.0	107.0
	θ(N1−N2−H2)	114.4	111.5
	θ(N2−N1−H3)	108.4	107.8
	θ(N2−N1−H4)	107.3	106.7
	θ(H3−N1−H4)	100.0	99.8
	θ(H5− H4−N1)	167.5	164.1
	Φ(H5−H4−N1−N2)	47.9	47.8

[a] TS denotes transition state.

are both gauche conformations with C_2 symmetry. Where comparison is possible, the theoretical bond lengths and bond angles for the reactants and the products at the UMP2/6-31+G(d,p) level are in good agreement with the experimental values.[38−40] Furthermore, the calculated structural parameters for all the stationary points at the UMP2/6-31+G(d,p) level of theory are close to those calculated at the higher level of QCISD/6-311G(d,p). For the transition state structures, the three atoms involved in the bond-breaking-and-bond-forming process are nearly collinear. At the UMP2/6-31+G(d,p) level of theory, the lengths of the breaking N−H bond in TS(a1), TS(a2), TS(b1), and TS(b2) increase by 17.4, 18.6, 17.4, and 18.6%, respectively, with respect to the corresponding equilibrium bond lengths of the reactant N_2H_4. Meanwhile, the lengths of the forming H−H bond in each transition state, which will form a hydrogen molecule, are ∼33.4, ∼31.5, ∼33.4, and 31.5% longer, respectively, than the equilibrium bond lengths of the hydrogen molecule. Therefore, all of the transition states are reactant-like, and the reactions will proceed via early transition states. This character is in accordance with the nature of exothermic reactions.[41]

Table 3 lists the harmonic vibrational frequencies and zero-point energies of the reactants, products, and transition states at the UMP2/6-31+G(d,p) level of theory along with the available experimental data.[42] It can be seen that the maximum error of the calculated frequencies is ∼11% compared with the experimental data. The frequencies calculated at the UMP2/6-31+G(d,p) level of theory and the ones calculated at the QCISD/6-311G(d,p) level of theory are similar. All the transition states have only one imaginary frequency. The absolute values of imaginary frequencies at the UMP2/6-31+G(d,p) level of theory for TS(a1), TS(a2), TS(b1), and TS(b2) are 2332, 2541, 2332, and 2541 cm^{-1}, respectively. The large values of imaginary frequencies imply that the tunneling correction is important for these reaction channels.

According to the optimized geometries discussed above, we can deduce that the four possible reaction channels are as follows:

$$N_2H_4(a) + H \rightarrow TS(a1) \rightarrow N_2H_3(a) + H_2 \tag{1}$$

$$N_2H_4(a) + H \rightarrow TS(a2) \rightarrow N_2H_3(a) + H_2 \tag{2}$$

$$N_2H_4(b) + H \rightarrow TS(b1) \rightarrow N_2H_3(b) + H_2 \tag{3}$$

$$N_2H_4(b) + H \rightarrow TS(b2) \rightarrow N_2H_3(b) + H_2 \tag{4}$$

The reaction enthalpies and potential barriers calculated at the four different levels of theory [UMP2/6-31+G(d,p), QCISD/6-311G(d,p), G2//QCISD/6-311G(d,p), and PMP4/6-311+G(3df,2pd)//UMP2/6-31+G(d,p)] are collected in Table 5. It can be seen that the reaction enthalpies of all the reaction channels at the latter two levels are very similar, and all of them are close to the corresponding experimental value of −21.09 kcal/mol derived from the experimental standard formation enthalpies (53.70 kcal/mol[43] for N_2H_3, 0.00 kcal/mol[44] for H_2, 22.77 kcal/mol[44] for N_2H_4, and 52.02 kcal/mol[44] for H).

In conclusion, we find that UMP2/6-31+G(d,p) and QCISD/6-311G(d,p) calculations can both provide accurate structural and frequency information, and G2//QCISD/6-311G(d,p) and PMP4/6-311+G(3df,2pd)//UMP2/6-31+G(d,p) calculations can effectively improve the potential energy. However, the combination of optimizing geometry at the UMP2/6-31+G(d,p) level of theory with refining energy at the PMP4/6-311+G(3df,2pd) level of theory is preferred due to its advantage in computational resources compared to the QCISD/6-311G(d,p) and G2//QCISD/6-311G(d,p) methods. Therefore, we adopted the PMP4/6-311+G(3df,2pd)//UMP2/6-31+G(d,p) method for the calculations of the four possible reaction channels. In addition, because of the mirror image equivalence between the reaction channels of reactions 1 and 3 as well as reactions 2 and 4, only kinetic data and figures of reactions 1 and 2 are provided.

B. Reaction Path Properties. The changes in the bond lengths and generalized normal mode vibrational frequencies of the four reactions along the MEPs as functions of intrinsic

TABLE 3: Harmonic Vibrational Frequencies (cm^{-1}) of the Equilibria and Transition States at the UMP2/6-31+G(d,p) and QCISD/6-311G(d,p) Levels and Zero-Point Energies (kcal/mol) at the UMP2/6-31+G(d,p) Level

	harmonic vibrational frequencies			
	UMP2/6-31+G(d,p)	QCISD/6-311G(d,p)	exptl[a]	ZPE
N_2H_4(a)	460, 861, 1016, 1147, 1321, 1353, 1712, 1732, 3556,3560, 3685, 3688	427, 907, 1071, 1153, 1337, 1371, 1689, 1711, 3490, 3504, 3602, 3608	371, 896, 914, 1035, 1284, 1285, 1579, 1598, 3274, 3293, 3334, 3336	34.4
N_2H_4(b)	460, 861, 1016, 1147, 1321, 1353, 1712, 1732, 3556, 3560, 3685, 3688	427, 907, 1071, 1153, 1337, 1371, 1689, 1711, 3490, 3504, 3602, 3608	371, 896, 914, 1035, 1284, 1285, 1579, 1598, 3274, 3293, 3334, 3336	34.4
N_2H_3(a)	577, 742, 1158, 1297, 1505, 1710, 3543, 3607, 3756	663, 756, 1156, 1246, 1514, 1684, 3444, 3543, 3664		25.6
N_2H_3(b)	579, 742, 1157, 1298, 1505, 1711, 3544, 3607, 3756	663, 756, 1156, 1246, 1514, 1684, 3444, 3543, 3664		25.6
H_2	4610	4423		6.6
TS(a1)	405, 432, 765, 879, 1093, 1195, 1270, 1426, 1566, 1584, 1717, 3541, 3550, 3700, 2332i	381, 385, 695, 931, 1069, 1167, 1259, 1419, 1541, 1604, 1700, 3490, 3508, 3619, 1710i		33.1
TS(a2)	309, 435, 659, 813, 1098, 1180, 1271, 1407, 1551, 1611, 1710, 3530, 3602, 3730, 2541i	219, 417, 616, 891, 1072, 1162, 1263, 1403, 1508, 1572, 1689, 3480, 3544, 3638, 2005i		32.7
TS(b1)	405, 432, 765, 879, 1093, 1195, 1270, 1426, 1566, 1584, 1717, 3541, 3550, 3700, 2332i	381, 385, 695, 931, 1069, 1167, 1259, 1419, 1541, 1604, 1700, 3490, 3508, 3619, 1710i		33.1
TS(b2)	309, 435, 659, 813, 1098, 1180, 1271, 1407, 1551, 1611, 1710, 3530, 3602, 3730, 2541i	219, 417, 616, 891, 1072, 1162, 1263, 1403, 1508, 1572, 1689, 3480, 3544, 3638, 2005i		32.7

[a] From ref 42.

TABLE 4: Total Energies (hartrees) for the Equilibria and Transition States

	UMP2/ 6-31+G(d,p)	QCISD/ 6-311G(d,p)	G2//QCISD/ 6-311G(d,p)	PMP4/6-311+ G(3df,2pd)// UMP2/ 6-31+G(d,p)
H	−0.4982329	−0.4998098	−0.4999998	−0.4998098
N_2H_4(a)	−111.5496599	−111.6062618	−111.6779267	−111.703693
N_2H_4(b)	−111.5496599	−111.6062618	−111.6779267	−111.703693
H_2	−1.1576611	−1.1683403	−1.165741	−1.1716651
N_2H_3(a)	−110.9125166	−110.970995	−111.0402373	−111.062518
N_2H_3(b)	−110.9125166	−110.970995	−111.0402383	−111.062518
TS(a1)	−112.0265192	−112.0950631	−112.1674309	−112.195308
TS(a2)	−112.022206	−112.0908833	−112.1640347	−112.191294
TS(b1)	−112.0265192	−112.0950631	−112.1674309	−112.195308
TS(b2)	−112.022206	−112.0908833	−112.1640357	−112.191294

TABLE 5: Reaction Enthalpies (ΔH°_{298}) and Potential Barriers (ΔE) (kcal/mol) for the Possible Reactions[a]

	reaction 1		reaction 2		reaction 3		reaction 4	
	ΔH°_{298}	ΔE	ΔH°_{298}	ΔE	ΔH°_{298}	ΔE	ΔH°_{298}	ΔE
UMP2[b]	−15.74	11.99	−15.74	14.48	−15.74	11.99	−15.74	14.48
QCISD[c]	−22.93	5.34	−22.93	7.68	−22.93	5.34	−22.93	7.68
G2//QCISD[d]	−19.66	5.02	−19.66	6.87	−19.66	5.02	−19.66	6.87
PMP4//UMP2[e]	−21.00	3.72	−21.00	6.02	−21.00	3.72	−21.00	6.02
				Experiment[f]				
	ΔH°_{298}					−21.09		
	E_a					2.5		

[a] Total energies (hartrees) of all the substances are listed in Table 4. [b] UMP2 denotes UMP2/6-31+G(d,p) + ΔZPE. [c] QCISD denotes QCISD/6-311G(d,p) + ΔZPE. [d] G2//QCISD denotes G2//QCISD/6-311G(d,p). [e] PMP4//UMP2 denotes PMP4/6-311+G(3df,2pd)//UMP2/6-31+G(d,p) + ΔZPE. [f] From ref 23.

reaction coordinates (amu$^{1/2}$ b) at the UMP2/6-31+G(d,p) level are shown in panels a and b of Figures 2 and 3, respectively. It can be seen that the changes are very similar for the four reaction channels. In panels a and b of Figure 2, the lengths of the breaking N−H bond and the forming H−H bond change significantly in the course of the reactions, while the other bond lengths change little. As the reaction proceeds to products, the length of the breaking N−H bond remains insensitive up to an s of -0.5 amu$^{1/2}$ b and then increases linearly. Meanwhile, the forming H−H bond rapidly shortens from that in reactants and arrives at the equilibrium bond length of the hydrogen molecule at an s of $\sim$0.5 amu$^{1/2}$ b.

In Figure 3, there are 15 vibrational frequencies near the transition state ($s = 0$). It is obvious that the vibrational frequency represented by a solid line changes strongly in the range of s from -0.5 to 0.5 amu$^{1/2}$ b. When $s < 0$ amu$^{1/2}$ b, this vibrational mode connects with the stretching vibration frequency of the breaking N−H bond of the N_2H_4 molecule; however, when $s > 0$ amu$^{1/2}$ b, the vibrational mode connects with the stretching vibrational frequency of the forming H−H bond of the H_2 molecule. In other words, from $s = -\infty$ to $s = \infty$, the vibrational mode changes from the stretching vibrational mode of the breaking N−H bond to the stretching vibrational mode of the forming H−H bond. This kind of behavior is known to be typical of hydrogen abstraction reactions. Therefore, from the changes in bond lengths and frequencies, the "reaction region" is in the s range of -0.5 to 0.5 amu$^{1/2}$ b.

Panels a and b of Figure 4 show the classical potential energy (V_{MEP}), the zero-point energy (ZPE), and the ground state vibrationally adiabatic potential energy (V_a^G) (the solid lines). For the four reaction channels, the position of the maximum value of the potential energy curve [$V_{\mathrm{MEP}}(s)$] at the PMP4/6-311+G(3df,2pd) level does not correspond to the saddle point position ($s = 0$) at the UMP2/6-31+G(d,p) level, but shifts slightly toward the reactant direction at an s of approximately -0.22 amu$^{1/2}$ b (the dotted line in panels a and b of Figure 4). This kind of shifting is caused by the computational technique.[45,46] To ensure the accuracy of the following steps, the maximum position for $V_{\mathrm{MEP}}(s)$ is shifted artificially to the saddle point position ($s = 0$) (the solid line in panels a and b of Figure 4). It should be noted that the maximum positions of V_a^G are very close to the maximum positions of V_{MEP}, and the two curves are similar in shape because the ZPE curve is practically constant as s varies with only a gentle fall near the saddle point ($s = 0$). This implies that the variational effect for the reactions will be small. In addition, it is obvious that the favorable possible reaction channels are reactions 1 and 3 according to the potential

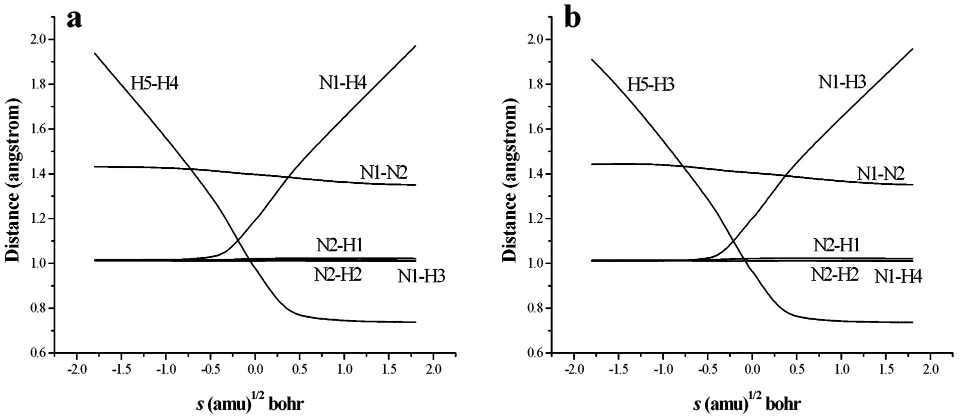

Figure 2. Changes in the bond lengths (Å) as functions of *s* (amu$^{1/2}$ b) at the UMP2/6-31+G(d,p) level: (a) reaction 1 (same as reaction 3) and (b) reaction 2 (same as reaction 4) (the labels of the bonds changing in reactions 3 and 4 can be seen in Figure 1).

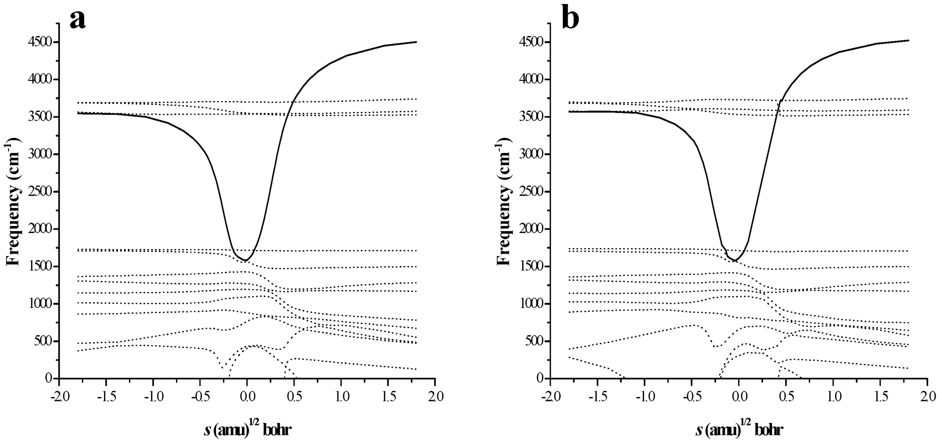

Figure 3. Changes in the generalized normal mode vibrational frequencies as functions of *s* (amu$^{1/2}$ b) at the UMP2/6-31+G(d,p) level: (a) reaction 1 (same as reaction 3) and (b) reaction 2 (same as reaction 4).

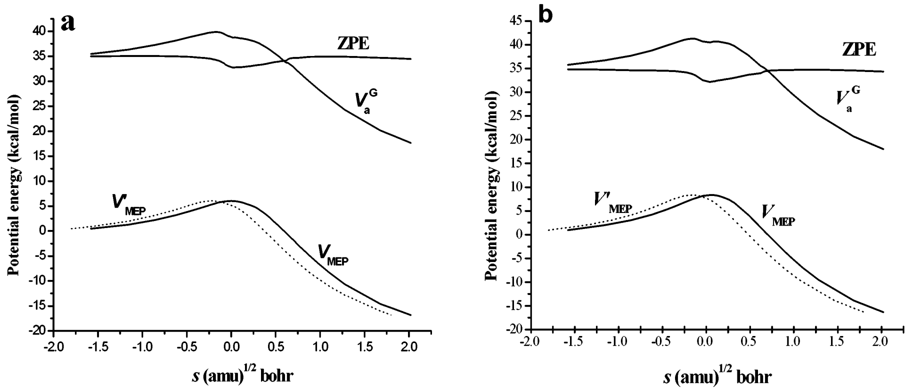

Figure 4. Classical potential energy (V_{MEP}), zero-point energy (ZPE), and ground state vibrationally adiabatic potential energy (V_a^G) as functions of *s* (amu$^{1/2}$ b) at the PMP4/6-311+G(3df,2pd)//UMP2/6-31+G(d,p) level: (a) reaction 1 (same as reaction 3) and (b) reaction 2 (same as reaction 4). The dotted line denotes the unshifted curve, and the solid line denotes the curve shifted artificially.

barrier heights taken from Figure 4. For a comprehensive understanding of the variational effect, the dynamics bottleneck properties of all the channels are listed in Table 6, in which only reactions 1 and 2 are discussed. It is shown that the positions of *s* of the variational transition state at various temperatures deviate little from the saddle point at $s = 0$. For both reactions 1 and 3, the deviation is largest at 3000 K, where it is 0.0723 amu$^{1/2}$ b, and the corresponding V_{MEP} and V_a^G values are 5.90 and 39.12 kcal/mol, respectively. For the classical transition state ($s = 0$), V_{MEP} and V_a^G equal 6.03 and 39.08 kcal/mol, respectively. The largest deviations are as follows: V_a^G ($s = 0.0723$) $-$ V_a^G ($s = 0$) $= 0.04$ kcal/mol and V_{MEP} ($s = 0.0723$) $-$ V_{MEP} ($s = 0$) $= -0.13$ kcal/mol for both channels, which are all very small. Thus, the variational effect for the calculation of the rate constant is very small.

C. Rate Constant Calculation. The rate constants of the reactions are calculated using the improved canonical variational transition state theory with the small curvature tunneling correction (ICVT/SCT) method at the PMP4/6-311+G(3df,2pd)//UMP2/6-31+G(d,p) level of theory within a wide temperature range of 220−3000 K, and the results are listed in Table 7. For the purpose of comparison, the conventional transition state theory (TST) and the improved canonical variational transition state theory (ICVT) are also applied in an

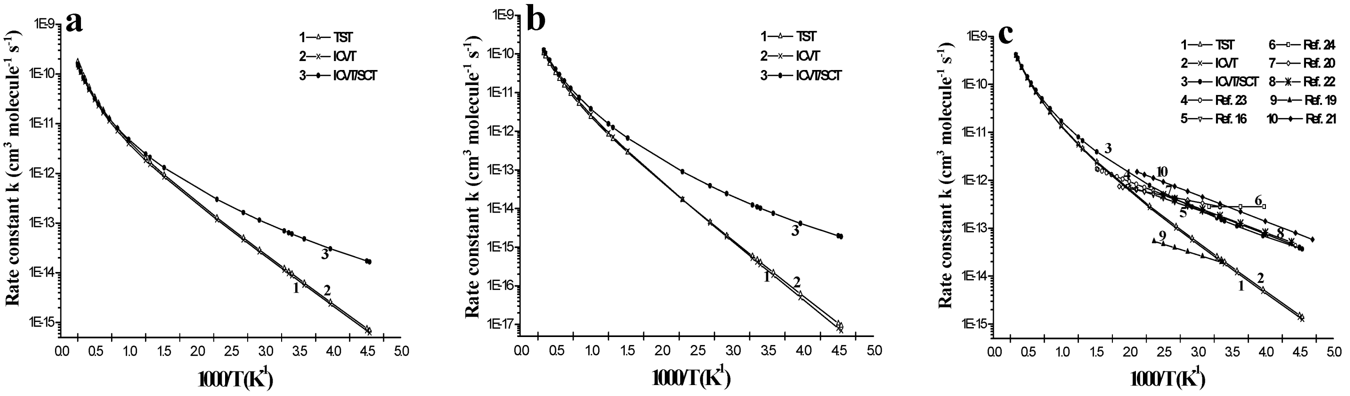

Figure 5. Plot of the IVCT/SCT rate constants, the TST rate constants, and the IVCT rate constants at the PMP4/6-311+G(3df,2pd)//UMP2/6-31+G(d,p) level, and the available experimental *k* values (cm^3 molecule^{-1} s^{-1}) vs 1000/*T* (K^{-1}) in the temperature range of 220−3000 K: (a) reaction 1 (same as reaction 3), (b) reaction 2 (same as reaction 4), and (c) sum of the four reaction channels.

TABLE 6: Dynamics Bottleneck Properties of the Four Reaction Channels Based on the ICVT Method

	reaction 1 or reaction 3			reaction 2 or reaction 4		
T (K)	s (amu$^{1/2}$ b)	V_{MEP} (kcal/mol)	V_a^G (kcal/mol)	s (amu$^{1/2}$ b)	V_{MEP} (kcal/mol)	V_a^G (kcal/mol)
SP	0.0000	6.03	39.08	0.0000	8.25	41.00
0.00	0.0634	5.93	39.12	0.0694	8.32	41.40
220.00	0.0640	5.93	39.12	0.0758	8.31	41.31
298.00	0.0654	5.92	39.12	0.0757	8.31	41.31
400.00	0.0674	5.92	39.12	0.0756	8.31	41.32
600.00	0.0692	5.91	39.12	0.0755	8.31	41.32
800.00	0.0700	5.91	39.12	0.0755	8.31	41.32
1000.00	0.0705	5.91	39.12	0.0754	8.31	41.32
1500.00	0.0713	5.91	39.12	0.0754	8.31	41.32
2000.00	0.0717	5.91	39.12	0.0754	8.31	41.32
2500.00	0.0720	5.90	39.12	0.0754	8.31	41.32
3000.00	0.0723	5.90	39.12	0.0754	8.31	41.32

effort to obtain the reaction rate constants in the same temperature range, and the results are also listed in Table 7. It can be seen from Table 7 that the rate constants of reaction 1 (or reaction 3) are larger than those of reaction 2 (or reaction 4) at <1400 K. However, at >1400 K, the rate constants of reaction 2 (or reaction 4) are larger than those of reaction 1 (or reaction 3). The total rate constants of reactions 1−4 are also listed in Table 7 and Figure 5c. It is obvious that the calculated total rate constants are well located between the experimental measurement in the whole temperature range where experimental data are available. However, we should note that even though the total ICVT/SCT values are in good agreement with the experimental values at <400 K, the total ICVT/SCT rate constants overestimate the experimental ones by a factor of approximately 3 at ≥400 K. This indicates that the small curvature tunneling correction has a smaller effect on reaction rate constants at high temperatures than at low temperatures. Therefore, the tunneling effect on the reaction rate constants is very important at low temperatures, while at high temperatures, it can be ignored.

To provide the best possible comparison with experiments, the activation energies of the reactions are calculated from fitting the ICVT/SCT rate constants to the Arrhenius expression in different temperature ranges, and the energies are listed in Table 8. Apparently, the results of reactions 1 and 3 are in good agreement with the experimental values reported by Vaghjiani et al.,[23] Gehring et al.,[21] and Stief and Payne,[22] respectively.

TABLE 7: Rate Constants (cm^3 molecule^{-1} s^{-1}) of Reactions 1−4 in the Temperature Range of 220−3000 K at the PMP4/6-311+G(3df,2pd)//UMP2/6-31+G(d,p) Level

	reaction 1 or reaction 3			reaction 2 or reaction 4			sum of ICVT/SCT	
T (K)	TST	ICVT	ICVT/SCT	TST	ICVT	ICVT/SCT	rate constant	exptl[a]
220	6.90×10^{-16}	6.24×10^{-16}	1.66×10^{-14}	9.33×10^{-18}	6.95×10^{-18}	1.88×10^{-15}	3.70×10^{-14}	
222	7.58×10^{-16}	6.85×10^{-16}	1.73×10^{-14}	1.07×10^{-17}	8.00×10^{-18}	1.98×10^{-15}	3.86×10^{-14}	4.01×10^{-14}
252	2.58×10^{-15}	2.35×10^{-15}	3.05×10^{-14}	6.21×10^{-17}	5.03×10^{-17}	4.12×10^{-15}	6.92×10^{-14}	$(0.83 \pm 0.09) \times 10^{-13}$
279	6.25×10^{-15}	5.70×10^{-15}	4.80×10^{-14}	2.21×10^{-16}	1.89×10^{-16}	7.50×10^{-15}	1.11×10^{-13}	$(1.09 \pm 0.12) \times 10^{-13}$
294	9.54×10^{-15}	8.70×10^{-15}	6.04×10^{-14}	4.05×10^{-16}	3.55×10^{-16}	1.02×10^{-14}	1.41×10^{-13}	$(1.50 \pm 0.18) \times 10^{-13}$
298	1.06×10^{-14}	9.67×10^{-15}	6.41×10^{-14}	4.72×10^{-16}	4.16×10^{-16}	1.10×10^{-14}	1.50×10^{-13}	$(1.58 \pm 0.24) \times 10^{-13}$[b]
304	1.24×10^{-14}	1.13×10^{-14}	6.99×10^{-14}	5.88×10^{-16}	5.23×10^{-16}	1.24×10^{-14}	1.65×10^{-14}	$(1.08 \pm 0.12) \times 10^{-13}$[c]
342	2.90×10^{-14}	2.65×10^{-14}	1.15×10^{-13}	2.00×10^{-15}	1.87×10^{-15}	2.42×10^{-14}	2.78×10^{-13}	$(1.80 \pm 0.18) \times 10^{-13}$[c]
372	5.05×10^{-14}	4.62×10^{-14}	1.63×10^{-13}	4.45×10^{-15}	4.27×10^{-15}	3.87×10^{-14}	4.03×10^{-13}	$(3.20 \pm 0.48) \times 10^{-13}$
435	1.29×10^{-13}	1.17×10^{-13}	3.01×10^{-13}	1.69×10^{-14}	1.70×10^{-14}	8.96×10^{-14}	7.81×10^{-13}	$(3.66 \pm 0.66) \times 10^{-13}$[c]
657	9.35×10^{-13}	8.46×10^{-13}	1.30×10^{-12}	2.80×10^{-13}	3.06×10^{-13}	6.61×10^{-13}	3.92×10^{-12}	1.72×10^{-12}
761	1.68×10^{-12}	1.51×10^{-12}	2.09×10^{-12}	6.31×10^{-13}	7.01×10^{-13}	1.25×10^{-12}	6.68×10^{-12}	$(21.3 \pm 4.9) \times 10^{-13}$
800	2.03×10^{-12}	1.83×10^{-12}	2.45×10^{-12}	8.17×10^{-13}	9.12×10^{-13}	1.55×10^{-12}	8.00×10^{-12}	
1000	4.46×10^{-12}	3.99×10^{-12}	4.82×10^{-12}	2.36×10^{-12}	2.68×10^{-12}	3.78×10^{-12}	1.72×10^{-11}	
1200	8.04×10^{-12}	7.15×10^{-12}	8.16×10^{-12}	5.12×10^{-12}	5.87×10^{-12}	7.47×10^{-12}	3.13×10^{-11}	
1400	1.28×10^{-11}	1.14×10^{-11}	1.25×10^{-11}	9.32×10^{-12}	1.08×10^{-11}	1.28×10^{-11}	5.06×10^{-11}	
1600	1.88×10^{-11}	1.66×10^{-11}	1.79×10^{-11}	1.51×10^{-11}	1.75×10^{-11}	2.00×10^{-11}	7.58×10^{-11}	
1800	2.61×10^{-11}	2.29×10^{-11}	2.43×10^{-11}	2.26×10^{-11}	2.62×10^{-11}	2.92×10^{-11}	1.07×10^{-10}	
2000	3.45×10^{-11}	3.03×10^{-11}	3.18×10^{-11}	3.19×10^{-11}	3.70×10^{-11}	4.04×10^{-11}	1.44×10^{-10}	
2400	5.48×10^{-11}	4.80×10^{-11}	4.96×10^{-11}	5.56×10^{-11}	6.46×10^{-11}	6.87×10^{-11}	2.37×10^{-10}	
2800	7.97×10^{-11}	6.95×10^{-11}	7.12×10^{-11}	8.64×10^{-11}	1.00×10^{-10}	1.05×10^{-10}	3.52×10^{-10}	
3000	9.36×10^{-11}	8.16×10^{-11}	8.34×10^{-11}	1.04×10^{-10}	1.21×10^{-10}	1.26×10^{-10}	4.19×10^{-10}	

[a] From ref 23. [b] From ref 14. [c] From ref 16.

TABLE 8: Forward Activation Energies (E_a) (kcal/mol) for the Title Reaction Calculated by ICVT/SCT Theory

temperature range (K)	reaction 1	reaction 2	reaction 3	reaction 4	exptl[a]
222−657	2.88	3.87	2.88	3.87	2.50 ± 0.04[b]
228−400	2.54	3.39	2.54	3.39	2.38 ± 0.10[c]
260−450	2.78	3.76	2.78	3.76	2.50 ± 0.20[d]
298−423	2.88	3.91	2.88	3.91	2.00[e]
305−505	3.06	4.16	3.06	4.16	2.22 ± 0.22[f]
657−886	4.79	6.41	4.79	6.41	4.70 ± 0.15[b]
220−3000	4.02	5.24	4.02	5.24	

[a] Experimental apparent activation energy. [b] From ref 23. [c] From ref 22. [d] From ref 21. [e] From ref 19. [f] From ref 16.

Summary

In this paper, the hydrogen abstraction reaction $N_2H_4 + H \rightarrow N_2H_3 + H_2$ has been investigated by an ab initio direct dynamics method. The results show that the UMP2/6-31+G(d,p) method can provide accurate geometry and frequency information compared with those obtained from the QCISD/6-311G(d,p) method. The calculations of single-point energies at the PMP4/6-311+G(3df,2pd)//UMP2/6-31+G(d,p) level of theory are necessary to improve the potential energy curve to obtain satisfactory reaction rate constants. The rate constants in the temperature range of 220−3000 K are calculated by using the improved canonical variational transition state theory with the small curvature tunneling correction (ICVT/SCT) method. The calculated results show that within the lower temperature range, the variational effect is small, and the small curvature tunneling effect is important. By comparison, the ICVT/SCT rate constants of reactions 1 and 3 in the lower experimentally measured temperature range at the PMP4/6-311+G(3df,2pd)//UMP2/6-31+G(d,p) level of theory are close to the measured values, and the total ICVT/SCT rate constants of all the reaction channels are in especially excellent agreement with the corresponding experimental data. It indicates that the four possible reaction channels caused by different N_2H_4 structures and different positions of hydrogen atom attack will all occur synchronously during the reaction, and among them, the most favorable reaction channels are reactions 1 and 3 in the lower temperature range. In the higher temperature range, the importance of reactions 2 and 4 becomes obvious, reactions 2 and 4 becoming even more important than reactions 1 and 3.

Acknowledgment. We thank Professor D. G. Truhlar for providing POLYRATE version 8.2. We also thank Dr. C. Y. Wang for his useful help.

References and Notes

(1) Sutton, G. P. *Rocket Propulsion Elements. An Introduction to the Engineering of Rockets*; Wiley: New York, 1992.

(2) Viereck, R. A.; Berstein, L. S.; Mende, S. B.; Murad, E.; Swenson, G. R.; Pike, C. P. *J. Spacecr. Rockets* **1993**, *30*, 724.

(3) Gray, P.; Lee, J. C.; Spencer, M. *Combust. Flame* **1963**, *7*, 315.

(4) Kaufman, F.; Gerri, N. J. *Proceedings of the Combustion Institute*; The Combustion Institute: Pittsburgh, PA, 1961; Vol. 8, p 619.

(5) Gray, P.; Lee, J. C. *Proceedings of the Combustion Institute*; The Combustion Institute: Pittsburgh, PA, 1955; Vol. 5, p 692.

(6) Auzanneau, M.; Roux, M. *Combust. Sci. Technol.* **1990**, *73*, 505.

(7) Heinrich, H. J. *Z. Phys. Chem. Neue Folge* **1964**, *42*, 149.

(8) Pedley, M. D.; Bishop, C. V.; Benz, F. J.; Bennett, C. A.; McClenagan, R. D.; Fenton, D. L.; Knystautas, R.; Lee, J. H.; Peraldi, O.; Dupre, G.; Shepherd, J. E. *AIAA Prog. Astronaut. Aeronaut.* **1988**, *114*, 45.

(9) Konnov, A. A.; Ruyck, J. D. *Combust. Flame* **2001**, *124*, 106.

(10) Moberly, W. H. *J. Phys. Chem.* **1962**, *66*, 366.

(11) Szwarc, M. *Proc. R. Soc. London, Ser. A* **1949**, *198*, 267.

(12) Genich, A. P.; Zhirnov, A. A.; Manelis, G. B. *Russ. J. Phys. Chem.* **1974**, *48*, 416.

(13) Diesen, R. W. *J. Chem. Phys.* **1963**, *39*, 2121.

(14) Vaghjiani, G. L. *J. Phys. Chem. A* **1997**, *101*, 4167.

(15) Ghosh, P. K.; Bair, E. J. *J. Chem. Phys.* **1966**, *45*, 4738.

(16) Chobanyan, S. A.; Mkryan, T. G.; Sarkisyan, E. N. *Kinet. Catal.* **1985**, *26*, 857.

(17) Schmidt, E. W. *Hydrazine and Its Derivatives: Preparation, Properties, Applications*; Wiley: New York, 1984.

(18) Birse, E. A. B.; Melville, H. W. *Proc. Royal Soc.* **1940**, *175*, 164.

(19) Schiavello, M.; Volpi, G. G. *J. Chem. Phys.* **1962**, *37*, 1510.

(20) Francis, P. D.; Jones, A. R. *J. Chem. Phys.* **1971**, *54*, 5085.

(21) Gehring, M.; Hoyermann, K.; Wagner, H. G.; Wolfrum, J. *Ber. Bunsen-Ges. Phys. Chem.* **1971**, *75*, 1287.

(22) Stief, L. J.; Payne, W. A. *J. Chem. Phys.* **1976**, *64*, 4892.

(23) Vaghjiani, G. L. *Int. J. Chem. Kinet.* **1995**, *27*, 777.

(24) Gehring, M.; Hoyermann, K.; Wagner, H. G.; Wolfrum, J. *Ber. Bunsen-Ges. Phys. Chem.* **1969**, *73*, 956.

(25) Truhlar, D. G.; Gordon, M. S. *Science* **1990**, *249*, 491.

(26) Garrett, B. C.; Truhlar, D. G.; Grev, R. S.; Magnuson, A. W. *J. Phys. Chem.* **1980**, *84*, 1730.

(27) Frisch, M. J.; Trucks, G. W.; Schlegel, H. B.; Scuseria, G. E.; Robb, M. A.; Cheeseman, J. R.; Zakrzewski, V. G.; Montgomery, J. A., Jr.; Stratmann, R. E.; Burant, J. C.; Dapprich, S.; Millam, J. M.; Daniels, A. D.; Kudin, K. N.; Strain, M. C.; Farkas, O.; Tomasi, J.; Barone, V.; Cossi, M.; Cammi, R.; Mennucci, B.; Pomelli, C.; Adamo, C.; Clifford, S.; Ochterski, J.; Petersson, G. A.; Ayala, P. Y.; Cui, Q.; Morokuma, K.; Malick, D. K.; Rabuck, A. D.; Raghavachari, K.; Foresman, J. B.; Cioslowski, J.; Ortiz, J. V.; Baboul, A. G.; Stefanov, B. B.; Liu, G.; Liashenko, A.; Piskorz, P.; Komaromi, I.; Gomperts, R.; Martin, R. L.; Fox, D. J.; Keith, T.; Al-Laham, M. A.; Peng, C. Y.; Nanayakkara, A.; Challacombe, M.; Gill, P. M. W.; Johnson, B.; Chen, W.; Wong, M. W.; Andres, J. L.; Gonzalez, C.; Head-Gordon, M.; Replogle, E. S.; Pople, J. A. *Gaussian98*; Gaussian, Inc.: Pittsburgh, PA, 1998.

(28) Hehre, W. J.; Ditchfield, R.; Pople, J. A. *J. Chem. Phys.* **1972**, *56*, 2257.

(29) Krishnan, R.; Binkley, J. S.; Seeger, R.; Pople, J. A. *J. Chem. Phys.* **1980**, *72*, 650.

(30) Pople, J. A.; Head-Gordon, M.; Raghavachari, K. *J. Chem. Phys.* **1987**, *87*, 5968.

(31) Schlegel, H. B. *J. Comput. Chem.* **1986**, *84*, 4530.

(32) Chuang, Y.-Y.; Corchado, J. C.; Fast, P. L.; Villa, J.; Hu, W.-P.; Liu, Y.-P.; Lynch, G. C.; Jackels, C. F.; Nguyen, K.; Gu, M. Z.; Rossi, I.; Coitino, E.; Clayton, S.; Melissas, V. S.; Lynch, B. J.; Steckler, R.; Garret, B. C.; Isaacson, A. D.; Truhlar, D. G. *POLYRATE*, version 8.2; University of Minnesota: Minneapolis, MN, 1999.

(33) Truhlar, D. G.; Isaacson, A. D.; Garret, B. C. *Theory of chemical reaction dynamics*; Baer, M., Ed.; CRC Press: Boca Raton, FL, 1985; Vol. 4, p 65.

(34) Steckler, R.; Hu, W. P.; Liu, Y. P.; Lynch, G. C.; Garrett, B. C.; Isaacson, A. D.; Melissas, V. S.; Lu, D. H.; Troung, T. N.; Rai, S. N.; Hancock, G. C.; Lauderdale, J. G.; Joseph, T.; Truhlar, D. G. *Comput. Phys. Commun.* **1995**, *88*, 341.

(35) Burenin, A. V. *Opt. Spectrosc.* **1999**, *86*, 34.

(36) Burenin, A. V. *Opt. Spectrosc.* **2000**, *88*, 28.

(37) Ding, F. J.; Zhang, L. F. *Int. J. Quantum Chem.* **1997**, *64*, 447.

(38) Kohata, K.; Fukuyama, T.; Kuchltsu, K. *J. Phys. Chem.* **1982**, *86*, 602.

(39) Tsunekawa, S. *J. Phys. Soc. Jpn.* **1976**, *41*, 2077.

(40) Tsuboi, M.; Overend, J. *J. Mol. Spectrosc.* **1974**, *52*, 256.

(41) Hammond, G. S. *J. Am. Chem. Soc.* **1963**, *85*, 3239.

(42) Yamaguchi, A. *Nippon Kagaku Zasshi* **1959**, *80*, 1109.

(43) Armstrong, D. A.; Yu, D.; Rauk, A. *J. Phys. Chem. A* **1997**, *101*, 4761.

(44) Wagman, D. D.; Evans, W. H.; Parker, V. B.; Schumm, R. H.; Halow, I.; Bailey, S. M.; Chumey, K. L.; Nuttall, R. L. NBS Tables of Chemical Thermodynamic Properties: Selected Values for Inorganic and C_1 and C_2 Organic Substances in SI Units. *J. Phys. Chem. Data* **1982**, *11*, Suppl. 2.

(45) Espinosa-Garcia, J.; Corchado, J. C. *J. Phys. Chem.* **1995**, *99*, 8613.

(46) Rosenman, E.; McKee, M. L. *J. Am. Chem. Soc.* **1997**, *119*, 9033.